Synthesis, Separation and Electrical Properties of WO_{3-x} Nanopowders via Partial Pressure High Energy Ball-Milling

A. Al Mohammad*

Nano-Materials Labs, Physics Department, Atomic Energy Commission of Syria

P.O. Box 6091, Damascus, Syria

Reduction processes of WO_3 nanopowder either with carbon or with hydrogen were observed using X-ray powder diffraction and transmission electron microscope. The phase transformations, separation, grain size and electrical conductivity of WO_{3-x} nanopowder during reductions via partial pressure high energy ball-milling have been studied. During the carbon-reduction process the monoclinic WO_3 structure transforms to nonstoichiometric Magneli phases $W_{40}O_{118}$, $WO_{2.9}$ and finally to WO_2 and W mixed phases. The Magneli WO_{3-x} phases exhibit specific fringe contrast imaging of well-ordered crystallographic shear planes. In comparison, the monoclinic WO_3 structure transforms to hydrate $WO_3 \cdot 1/3H_2O$, hexagonal WO_3, non-stoichiometric $WO_{2.7}$ and finally to WO_2 and W mixed phases during the hydrogen-reduction process. The inclusion of hydrogen atoms between the WO_6 octahedral structure shifts the reduction steps to lower milling times. It demonstrates that the formation of hydrate WO_3 phases enhances the amenability of the system to reduction. The activation energy for conduction was deduced from the Arrhenius equation and was found to depend on oxygen partial pressure or presence of the hydrogen atoms. The defect band model was used for interpretation of these behaviors. It supposes that the surface oxygen vacancies introduce donor levels in the gap of semiconductor, so free electrons are produced by reduction.

PACS numbers: 81.20.Ev, 61.46.Df, 64.60.Cn

1. Introduction

In the current materials science research, great emphasis has been placed on the nanosized materials in order to study the unique physical properties that are derived from size reduction effects down to the nanodimension [1–3]. The surface-to-bulk ratio for the nanosized materials is much greater than that for coarse materials. In nanosized materials, a large fraction of the atoms is present at the surface, and hence, the surface properties become paramount. Another important factor associated with the depth of the surface space charge region is affected by the relation between gas adsorption and the particle size. These characteristics of nanosized particles make the materials particularly appealing in their applications as gas sensors. Indeed, grain-size reduction is one of the main factors in enhancing the gas sensing properties of semiconducting oxides. The use of nanosized materials in gas sensors is rapidly going interest in the scientific community [2–4]. The gas sensors using metal oxide semiconductors (MOSs) have been put into practice for various fields of applications because of their advantageous features such as the simple device structure, the

fairly high sensitivity and the excellent stability. Yet full capability of this group of sensors has not been exploited sufficiently. It has been recognized fairly well that their gas-sensing mechanism consists of receptor function and transducer function [5–7].

Nanosized powders for gas sensor applications have been prepared using various methods, including the sol–gel process, chemical co-precipitation and metal–organic decomposition (MOD) [8–12]. Besides these methods, the high-energy ball milling or mechanical alloying has proven to be a very effective route in preparing nanosized solid solution for gas sensing applications [13–16]. The alloying process can be carried out using different apparatus, namely, planetary mills, horizontal ball mills or vibration mills. However, in comparison to other milling methods, the short milling times of synthesis contribute to become the planetary ball mills which are frequently used in mechanical alloying and mechanical activation processes.

Non-stoichiometric tungsten oxides (WO_{3-x} where $0 \leq x \leq 3$) as thin films or nanopowders (NPs) have been studied because of their potential applications in MOS gas sensor devices [10–14] such as electrochromic devices (ECDs) solar panel arrays and smart windows. Generally, the majority of the WO_3 sensing properties are connected with: (1) the WO_3 structural model is perovskite-

* e-mail: scientific@aec.org.sy

(240)

-type ABO$_3$ lattice with A site, which remains an unoccupied site; (2) the WO$_3$ is considered as oxygen-deficient or non-stoichiometrical oxide represented by WO$_{3-x}$, where x depends on the sample treatments. Using the high-energy ball milling process, stable WO$_{3-x}$ NPs with grain sizes down to a few nanometers can be obtained at room temperature. However, there have been scarce scientific reports into the electrical characterization of dense WO$_{3-x}$ NPs with regards to their milling process and nanostructure.

In this work, two new reduction processes of WO$_3$ nanopowder either with carbon or with hydrogen were achieved. The partial pressure high energy ball-milling (PPHEBM) technique has been employed to synthesize various stable phases of the WO$_{3-x}$ NPs during reductions of monoclinic WO$_3$ powder. Hydrogen gas or active carbon is used as additive element of reduction reactions. The nanostructure of synthesized WO$_{3-x}$ NPs and their associated effects on electrical properties of WO$_{3-x}$ NPs have been characterized.

2. Experimental

High-purity WO$_3$ powder (WO$_3$, 99% purity, 20 μm, Aldrich, Germany) was used as a raw material. Two processes of PPHEBM of WO$_3$ powder were carried out using variable planetary mill (Activator 2S, Russia). The starting materials of the first process were a mixture of WO$_3$ powder and commercial active carbon in 2:3 molar ratio. The mill jars were closed under vacuum less than 100 Pa of Ar. The second process was a reduction reaction of WO$_3$ powder by milling under 100 Pa of 7% H$_2$ in high-purity Ar. All jars were closed in a vacuum chamber. It had a pressure less than 10^{-4} Pa before injection the mixture of H$_2$ and Ar gases. The samples of the first and second processes were named A and B, respectively. The milling conditions and the material compositions are summarized in Table I.

TABLE I

Milling conditions in the partial pressure high energy ball mill.

Reduction process	Raw materials	Adding gas	Pressure [Pa]	Materials of jars & balls	Ball to powder weight ratio	Volumes of jars [ml]	Ball diameters [mm]	Disc speed [rpm]	Jar speed [rpm]
A	WO$_3$ + C	Ar	100 Pa	WC	1:20	80	10	500	900
B	WO$_3$ + H$_2$	Ar	100 Pa	WC	1:20	80	10	500	900

The nanostructure and the phase transformations of WO$_{3-x}$ NPs were carried out using a transmission X-ray diffractometer (XRD) (Stoe, Germany) with Cu K monochromatized radiation. The XRD patterns of the NPs were recorded using a step size of 0.02° and a counting time of 5 s per step. A transmission electron microscope (TEM) (Siemens102, acceleration voltage 125 kV) and its selected area electron diffraction (SAED) were used for nanostructural studies.

WO$_{3-x}$ NP of each stable phase was ground in an agate mortar for 4 h in absolute ethanol. The NPs were pressed in cylindrical discs of about 10 mm diameter and 0.5 mm thickness at a pressure of 100 MPa. The discs were heated in residual oxygen pressure at about 0.1 Pa and a heating rate of 10 K/min up to the temperature of I–V measurement. The procedure was repeated at least twice to ensure that the crystallographic structure of the NP is stable as ascertained by powder X-ray diffraction and TEM. The conductivity measurements were carried out in removable reactors of pressure-controlled chamber during annealing the discs. The resistances of the discs were measured by the two-probes method and using interdigitated gold electrodes deposited on the disc by

electron gun deposition method (Elltrorava, Italy). The nature of the contact was verified to be ohmic by I–V measurements. A thermocouple was attached to the disc holder for monitoring and controlling the operation during conductance measurements.

3. Results and discussion

The X-ray powder diffraction patterns recorded during various periods of high energy ball milling of WO$_3$ oxide in processes A and B are shown in Fig. 1. Generally, the X-ray patterns of the starting materials showed only the Bragg reflections of monoclinic WO$_3$ (space group). During milling the structure and the grain size of WO$_3$ powders change considerably. X-ray patterns show a gradual broadening and simultaneous decrease in intensity of the lines; characteristic of the reduced WO$_3$ powders. The reduced WO$_2$ and W phases are more rapidly formed by milling in process A as compared to B. XRD patterns demonstrate that the kinetics of the milling process are complex and sensitive to the composition of the reactant mixtures. From these data we have inferred that the reductions of WO$_3$ powders with carbon occur in three

main milling times 0–70, 70–110 and 110–160 min, while there are four main milling times 0–30, 30–50, 50–74, and 74–100 min for the reduction process B. All XRD peaks were observed to broaden with increasing milling time in both processes A and B. The broadening was very rapid during the first milling time, but was quite marginal after that. The size variation of milled NPs was quantitatively calculated using the Scherrer formula [13, 17] and also observed by TEM [18]. Both methods showed consistent results, as presented in Fig. 2. The particle size decreased drastically to less than 20 nm after the first milling time and remained about the same size up to final milling time. The previous XRD results have been confirmed using TEM and SAED analysis. The reduction schemes and TEM with its SAED observations at several milling times of WO$_3$ NPs in processes A and B are shown in Fig. 3.
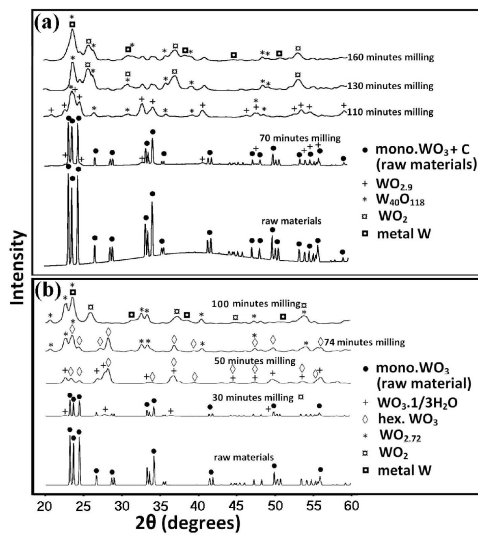
Fig. 1. X-ray diffraction patterns for the WO$_3$ nanopowders during phase transformations via high energy ball milling using: (a) carbon as adding materials, (b) H$_2$ as adding materials.
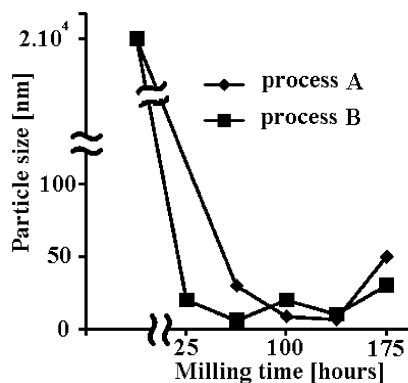
Fig. 2. Size variation of milled WO$_3$ NPs using processes A and B.
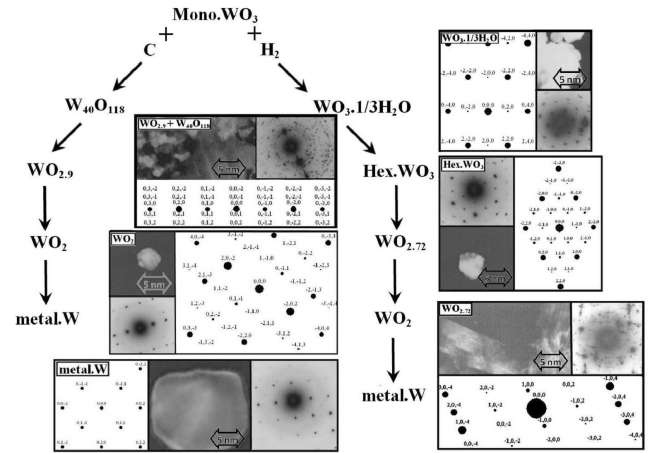
Fig. 3. The reduction schemes, TEM with its SAED observations at several milling times of WO$_3$ NPs in processes A and B.

The observed DC electrical conductivity of WO$_3$ NPs acts as the polycrystalline n-type semiconductor behaviour [19–22] with an activation energy of about 0.56(2) eV. Figure 4 represents the variation of activation energy σ of WO$_3$ NPs using milling processes A and B at the stable WO$_{3-x}$ phases. It is noted that the I–V data were measured at different WO$_{3-x}$ phases with about 97% of measured phase and 3% of adjoining phases. The conductivity is calculated from the experimentally determined resistance R, which is monitored during the three heating and cooling cycles. The activation energy of conduction, E_A, was frequently interpreted using the Arrhenius equation between 300 and 700 K. Our results are compatible with the principle results of conductivity of WO$_{3-x}$ thin films [19–26]. It is obtained from the following formula:

$$d(\log \sigma)/d(1/T) = -E_A/k, \qquad (1)$$

where k is Boltzmann's constant, T is the absolute temperature and σ is the variation of conductivity. The overall results of conductivity properties of the stable phases of processes A and B samples are grouped in Table II.

Using milling, XRD, TEM and SAED analyses shows that there is an increase in the degree of lattice disorder and a decrease in the crystallite size, thereby reducing the symmetry of the unit cell until some fraction of the material becomes at NP. As reported previously [27–29], the mechanical activation resulted in the NP of minerals, development of large numbers of dislocation and their associated strain fields, which decrease the crystallite size and change the lattice parameters. These dislocations might lead to an overall decrease in long range lattice periodicity. This may be interpreted as the formation of metastable "NP phases", because line broadening and reduction of diffraction peaks intensity take place on X-ray pattern after prolonged milling. In our case there are important changes in reduction processes of WO$_3$ NPs during milling as a function of additive materials.
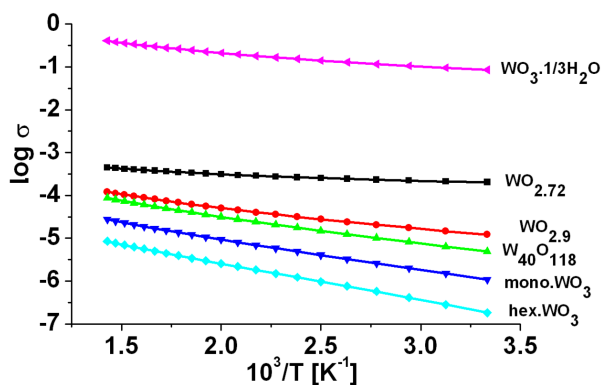
Fig. 4. Conductivity σ of the stable WO$_3$ nanopowder phases of milling processes A and B as a function of the reciprocal temperature (in a $\log \sigma$ versus $10^3/T$ plot) during heating cycle.

TABLE II

Variation of activation energy of WO$_3$ nanopowders after milling in several times.

Crystalline phase of WO$_3$ nanopowders	Activation energy [eV]	Electrical behavior
mono WO$_3$	0.82(4)	polycrystalline semiconductor
WO$_3\cdot1/3$H$_2$O	0.49(2)	metal-like
W$_{40}$O$_{118}$	0.77(3)	n-type semiconductor
WO$_{2.72}$	0.28(3)	n-type semiconductor
hex. WO$_3$	0.91(4)	semiconductor
WO$_{2.9}$	0.66(3)	n-type semiconductor
WO$_2$	–	metal-like
metal W	–	metallic

In case of process A, the milling of WO$_3$ NPs with carbon at a longer time than 30 min exhibit WO$_{3-x}$ with CS structures. These observations emphasize the role of carbon during recrystallisation of WO$_3$ NPs. Carbon has two main effects: (1) it reacts with O anions of WO$_6$ octahedral to produce CO gas and CS planes are easily formed. (2) Carbon can react with two O anions from two WO$_3$ NPs, so the grain size of WO$_{3-x}$ NPs increases. This does not mean that defects resulting from oxygen deficiency do not exist in smaller grains. However, they are probably only embryonic, with no specific contrast in TEM and no well-defined diffraction spots in SAED. In all cases, formation of CS planes gives a new atomic coordination, in which the WO$_6$ octahedra share their edges with W^{6+} species and are reduced to W^{5+}. The final structure of WO$_3$ observed in process A is the WO$_2$ monoclinic structure with metallic W.

In case of process B, inclusion of hydrogen atoms into the WO$_6$ octahedral structure shifts the reduction steps to lower milling times and enhances the amenability of the system to reduction. Also inclusion of hydrogen atoms makes the reduction process more complex. WO$_3$ and WO$_x$ NPs formed hexagonal or as-hexagonal structures.

It has been observed that during the first milling time, the conductivity value undergoes large variations, which could be explained either by structural modification effects (process A) [19] or by hydrogen interaction with WO$_6$ octahedral (process B). In WO$_{3-x}$ NPs with CS phases, we suppose that the conductivity of tungsten oxide NPs is governed by the non-stoichiometry of WO$_3$ considered as n-type semiconductor and assumed that the non-stoichiometry originates only from oxygen vacancies of WO$_6$ octahedral. The conductivity curve exhibits a slope similar to the one obtained for annealing WO$_3$ thin films in low oxygen pressure [19–23]. This indicates that the NPs keep the same structure characterized by a high density of oxygen vacancies [20–24]. While in process B, the activation energy E_A of WO$_3\cdot1/3$H$_2$O hydrate NPs corresponds obviously to a metal like behavior with $E_A = 0.49(2)$ eV. The conductivity of hexagonal phase becomes lowest and activation energy becomes the largest value, $E_A = 0.91(4)$ eV. The conductivity further increases and the value of activation energy of WO$_{2.7}$ NP is about $0.28(3)$ eV which corresponds to n-type semiconductor-like behavior. Results of WO$_3$ NPs conductivities and their interpretations as non-stoichiometric (process A) and hydrate (process B) originates from oxygen vacancies and are compatible with similar works that have been carried out in study of WO$_3$ thin films as a sensing material for detection of atmosphere pollutants [25–31].

4. Conclusions

During milling, the grain size of WO$_3$ powders decreased rapidly to nanosize (nanopowders). Therefore, the specific surface areas of NPs considerably increased. Also, the porosities of NPs increased in the range 10–30 nm. Reductions of WO$_3$ powders with carbon occur in three main milling times, with a global time of 160 min while hydrogen reduction process exhibited five main milling times with global time of 100 min. The very large contact surfaces between WO$_3$ NPs and added materials, the self-propagating nature of reduction allows for very short reduction times. Measurements of electrical conductivity of reduced materials during reduction provide a particular sensitive tool to monitor the structural changes of WO$_x$ NPs. Huge changes of the conductivity were observed from n-type semiconducting to as-metallic behaviour [32].

Acknowledgments

port and encouragement, as well as Prof. M.K. Sabra, M. Rukiah and M. Naddaf for valuable discussions.

References

[1] Gil-Su Kim, Young Jung Lee, Dae-Gun Kim, Young Do Kim, *J. Alloys Comp.* **454**, 327 (2008).

[2] Dae-Gun Kima, Kyung Ho Mina, Si-Young Changb, Sung-Tag Ohc, Chang-Hee Lee, Young Do Kima, *Mater. Sci. Eng. A* **399**, 326 (2005).

[3] Yu.M. Solonin, O.Yu. Khyzhun, E.A. Graivoronskaya, *Cryst. Growth Design* **1**, 473 (2001).

[4] C.V. Ramana, S. Utsunomiya, R.C. Ewing, C.M. Julien, U. Becker, *J. Phys. Chem. B* **110**, 10430 (2006).

[5] H. Meixner, J. Gerblinger, U. Lampe, M. Fleischer, *Sensors Actuators B* **23**, 119 (1995).

[6] Z.G. Huanga, Z.P. Guoa, A. Calka, D. Wexler, C. Lukeyc, H.K. Liu, *J. Alloys Comp.* **422**, 299 (2006).

[7] Gwan-Hyoung Lee, Shinhoo Kang, *J. Alloys Comp.* **419**, 281 (2006).

[8] M.C. Yang, J. Xu, Z.Q. Hu, *Int. J. Refractory Metals Hard Mater.* **22**, 1 (2004).

[9] Zhen Xiong, Gangqin Shao, Xiaoliang Shi, Xinglong Duan, Li Yan, *Int. J. Refractory Metals Hard Mater.* **26**, 242 (2008).

[10] W.J. Rankin, J.R. Wynnyckyj, *Metall. Mater. Trans. B* **28**, 308 (April 1997).

[11] A. Galembeck, O. L. Alves, *Thin Solid Films* **365**, 90 (2000).

[12] S. Sathyamurthy, K. Salama, *Physica C* **34**, 12479 (2000).

[13] A. Al Mohammad, *Phys. Status Solidi A* **205**, 2880 (2008).

[14] O.K. Tan, W. Zhu, Q. Yan, L.B. Kong, *Sens. Actuators B* **65**, 361 (2000).

[15] O.K. Tan, W. Cao, W. Zhu, *Sens. Actuators B* **63**, 129 (2000).

[16] Z. Ling, C. Leach, *Sens. Actuators B* **102**, 102 (2004).

[17] Shunji Abe, U-Sung Choi, Kengo Shimanoe, Noboru Yamazoe, *Sens. Actuators B* **107**, 516 (2005).

[18] V. Guidi, M. Blo, M.A. Butturi, M.C. Carotta, S. Galliera, A. Giberti, C. Malagù, G. Martinelli, M. Piga, M. Sacerdoti, B. Vendemiati, *Sens. Actuators B* **100**, 277 (2004).

[19] M. Gillet, K. Aguir, C. Lemire, E. Gillet, K. Schierbaum, *Thin Solid Films* **467**, 239 (2004).

[20] C. Cantalini, W. Wlodarski, Y. Li, *Sens. Actuators B, Chem.* **64**, 182 (2000).

[21] D.W. Bullett, *J. Phys. C, Solid State Phys.* **16**, 2197 (1983).

[22] C. Scott, S. Ding, R.J. Lad, *Sens. Actuators B* **77**, 375 (2001).

[23] M. Gillet, C. Lemire, E. Gillet, K. Aguir, *Surf. Sci.* **532/535**, 519 (2003).

[24] Q. Wang, Z. Wen, Y. Jeong, J. Choi, K. Lee, J. Li, *Nanotechnology* **17**, 3116 (2006).

[25] S.K. Deb, *Phys. Rev. B* **16**, 1020 (1977).

[26] A. Wolcott, T.R. Kuykendall, W. Chen, S. Chen, J.Z. Zhang, *J. Phys. Chem. B* **110**, 25288 (2006).

[27] H. Kawasaki, J. Namba,K. Iwatsuji, *Appl. Surf. Sci.* **197**, 547 (2002).

[28] S.C. Moulzoff, L.J. Legore, R.J. Lao, *Thin Solid Films* **400**, 56 (2001).

[29] M. Gillet, R. Delamare, E. Gillet, *J. Crystal Growth* **279**, 93 (2005).

[30] G.V. Kunte, U. Ail, *Bull. Mater. Sci.* **28**, 243 (2005).

[31] O.Yu. Khyzhum, *J. Alloys Comp.* **305**, 1 (2000).

[32] The crystallographic data can be obtained from following references and the Cambridge Crystallographic Data Centre (CCDC), `www.ccdc.cam.ac.uk`, 12, Union Road, Cambridge CB21EZ, UK.